Title
Carrier Lifetimes in a III-V-N Intermediate-Band Semiconductor

Journal
Physical Review Applied, 7(1)

ISSN
2331-7043

Authors
Heyman, JN
Schwartzberg, AM
Yu, KM
et al.

Publication Date
2017

DOI
10.1103/physrevapplied.7.014016

Peer reviewed

Carrier Lifetimes in a *III-V*-N Intermediate-Band Semiconductor

J. N. Heyman,[1,*] A. M. Schwartzberg,[2] K. M. Yu,[2,3] A. V. Luce,[2,4] O. D. Dubon,[2,4] Y. J. Kuang,[5] C. W. Tu,[5] and W. Walukiewicz[2]

[1]*Physics Department, Macalester College, St. Paul, Minnesota 55105, USA*
[2]*Materials Sciences Division, Lawrence Berkeley National Laboratory, Berkeley, California 94720, USA*
[3]*Department of Physics and Materials Science, City University of Hong Kong, Hong Kong SAR, China*
[4]*Department of Materials Science and Engineering, University of California, Berkeley, California 94720, USA*
[5]*Department of Physics, University of California, San Diego, California 92093, USA*

(Received 18 August 2016; revised manuscript received 21 October 2016; published 24 January 2017)

We use transient absorption spectroscopy to measure carrier lifetimes in the multiband semiconductor $GaP_yAs_{1-x-y}N_x$. These measurements probe the electron populations in the conduction band, intermediate band, and valence band as a function of time after an excitation pulse. Following photoexcitation of $GaP_{0.32}As_{0.67}N_{0.01}$, we find that the electron population in the conduction band decays exponentially with a time constant $\tau_{CB} = 23$ ps. The electron population in the intermediate band exhibits bimolecular recombination with recombination constant $r = 2 \times 10^{-8}$ cm^3/s. In our experiment, an optical pump pulse excites electrons from the valence band to the intermediate and conduction bands, and the change in interband absorption due to absorption saturation and induced absorption is probed with a delayed white-light pulse. We model the optical properties of our samples using the band anticrossing model to extract carrier densities as a function of time. These results not only identify the short minority-carrier lifetime as a key factor affecting the performance of $GaP_yAs_{1-x-y}N_x$-based intermediate-band solar cells but also provide guidance on ways to address this issue.

DOI: 10.1103/PhysRevApplied.7.014016

I. INTRODUCTION

Dilute *III-V* nitrides (*III-V*$_{1-x}$-N$_x$ with x less than approximately 5%) are termed highly mismatched alloys because the size and electronegativity of the N atoms differ strongly from those of the group-*V* host atoms. These materials have been successfully described by the band anticrossing model (BAC) [1,2], which predicts that the interaction between the extended conduction-band states of the host material and the localized energy states of the isoelectronic nitrogen impurities splits the conduction band into a distinct upper band (E_+) and lower band (E_-) separated by a gap. For example, studies of $GaAs_{1-x}N_x$ have shown [2–5] that the band anticrossing model can explain the strong dependence of the band gap and electron effective mass on nitrogen doping. Photomodulated reflection measurements have been used to identify the minima of the E_+ and E_- bands in $GaAs_{1-x}N_x$ and show that they shift with nitrogen concentration and hydrostatic pressure as predicted by the BAC model. Other *III-V* dilute nitrides including [1,2,6,7] $Ga_{1-y}In_yAs_{1-x}N_x$, $GaP_{1-x}N_x$, $GaSb_yAs_{1-x-y}N_x$, and $GaP_yAs_{1-x-y}N_x$ have been investigated and successfully described using the BAC model.

Dilute *III-V* nitrides are promising materials for intermediate-band solar cells (IBSCs). In the intermediate-band concept [8–10], solar photons excite electrons to the conduction band through two processes: direct excitation from the valence band to the conduction band (VB-E_+) or stepwise excitation from the valence band to the intermediate band (VB-E_-) and then to the conduction band (E_--E_+). By adjusting the material composition, these three transitions can be matched to the solar spectrum to efficiently capture solar energy. In an IBSC, the intermediate-band material is inserted into a *p-n* junction with the band gap matching the VB-E_+ gap so that photoelectrons and holes are extracted from the conduction band (E_+) and valence band. In principle, an intermediate-band solar cell possesses the advantages of a three-junction solar cell in a simpler device architecture. While the Shockley-Queisser efficiency limit for a single-junction photovoltaic device in concentrated sunlight is 41%, the limit for an intermediate-band solar cell is predicted [8] to be 63%. Intermediate-band solar cells have been implemented using $GaAs_{1-x}N_x$ [11] and (Zn,Te)O [12] highly mismatched alloys and by using quantum-dot arrays inserted into a *III-V* host material [13]. The status of the IBSC field has been recently reviewed by Okada *et al.* [10].

Recently, Lopez *et al.* [11] reported an IBSC based on $GaAs_{0.976}N_{0.024}$. Photocurrent spectra clearly show response associated with the VB-E_- and VB-E_+ transitions. Photocurrent generation by sequential excitation (VB-E_- followed by E_--E_+) has also been observed [14] in

*heyman@macalester.edu.

$GaAs_{1-x}N_x$, and the E_+-E_- transition has been observed in electroluminescence [15]. The efficiency of Lopez's prototype device was relatively low, and the open-circuit output voltage (0.9 V) was below prediction (approximately 1.6 V). The authors suggested that the low output voltage likely results from short minority-carrier lifetimes. In $GaAs_{1-x}N_x$, the BAC theory predicts the formation of a wide intermediate band with a finite density of states between the E_- and E_+. These gap states may be a pathway for rapid electron relaxation from the conduction band to the intermediate band. We also note that the energy-band positions in (Ga,As)N are not well matched to the solar spectrum.

In $ZnTe_{1-x}O_x$, the addition of oxygen at low concentrations produces a narrow band of oxygen-derived extended states below the conduction-band edge of ZnTe. This intermediate band can be described well by the BAC model [16]. Tanaka *et al.* [12,17] demonstrated a $ZnTe_{1-x}O_x$ IBSC. They used photomodulated reflectance measurements to determine the critical energies of the VB-E_-, VB-E_+, and E_--E_+ transitions. Photocurrent spectra of their device showed distinct photocurrent generation from VB-E_- and VB-E_+ transitions. The external quantum efficiency was low, and the open-circuit output voltage (0.36 V) was much lower than predicted (approximately 2 V). While these prototype IBSC devices are an important proof of principle, further developments are required to make the IBSC concept viable. Significant improvements may result from optimizing absorption in the intermediate-band material to match the solar spectrum and by improving carrier lifetimes.

$GaP_yAs_{1-x-y}N_x$ quaternary alloy is a promising material for implementing the IBSC concept [18]. A material with a P alloy fraction of approximately 40% and N fraction of approximately 2% is predicted to provide a nearly optimum band structure for solar-energy production. The nitrogen defect level in this material lies near or below the conduction-band minimum in the host material so that the anticrossing interaction produces a narrow N-derived intermediate band that is well separated from conduction band. Kuang *et al.* [19] recently grew $GaP_yAs_{1-x-y}N_x$ thin films on GaP substrates with gas-source molecular-beam epitaxy. Photomodulated reflectance (PR) measurements found VB-E_- and VB-E_+ transitions close to transition energies predicted by the BAC model [7]. Optical transmission measurements showed strong VB-E_- absorption. However, VB-E_+ transitions were not observed in transmission because the GaP substrates strongly absorb in this spectral region. Also, intermediate-band to conduction-band transitions (E_--E_+) were not observed in absorption or PR because these require population of the intermediate band.

Carrier dynamics in $GaP_yAs_{1-x-y}N_x$ have recently been investigated by Baranowski *et al.* [20] using time-resolved photoluminescence. They report luminescence near the VB-E_- absorption edge and measure luminescence lifetimes of approximately 100 ps at room temperature. The lifetimes increase dramatically as the temperature is reduced, reaching approximately 50 ns at $T < 100$ K. The authors describe the temperature-dependent luminescence using a hopping-exciton model: Excitons form after photoexcitation and are rapidly localized. Thermally activated hopping moves excitons between shallow localized states and deep nonradiative recombination centers. At high temperatures, all trap sites are accessible, and the deep nonradiative recombination sites dominate recombination. At low temperatures, excitons trapped in shallow localized states are protected from the deep traps, and long luminescence lifetimes are observed. This work does not determine the conduction-band carrier lifetime because the luminescence initiating in the conduction band is not observed. Also, luminescence primarily probes the dynamics of excitons rather than free carriers and can be dominated by defect-bound excitons.

In this paper, we use time-resolved optical absorption to investigate free-carrier dynamics in two $GaP_yAs_{1-x-y}N_x$ samples with compositions close to optimum for solar-energy collection. The samples are selected having unperturbed conduction bands slightly below (S205B) or slightly above (S376B) the N-defect level. Transient absorption primarily probes carriers in the bands and can determine carrier populations and distribution functions. We observe saturation of the VB-E_- and VB-E_+ transitions, as well as induce absorption at the E_--E_+ transition energy due to the optical population of the intermediate band. This allows us to find the carrier populations following photoexcitation and determine photocarrier lifetimes in the conduction and intermediate bands.

II. THEORETICAL MODEL

The dilute III-V_{1-x}-N_x alloy semiconductors studied here have been described in terms of a two-level BAC model (Table I) [1,2,21]. The model can be derived from the multi-impurity Anderson model in the coherent potential approximation. In this model, the restructuring of the conduction band results from the interaction between localized N orbitals and extended conduction-band states of the semiconductor host. The main effect of the interaction is to split the conduction band into E_+ and E_- bands separated by a gap. The conduction- and intermediate-band energies at wave vector k, E_k^+, and E_k^- are found from perturbation theory:

$$E_k^{\pm} = \frac{1}{2}[E_k^c + E_N \pm \sqrt{(E_k^c - E_N)^2 + 4V^2x}], \qquad (1)$$

where E_k^C is the unperturbed conduction-band energy at wave vector k, E_N is the energy of the nitrogen defect state, V is the interaction strength, and x is the nitrogen fraction. The calculated energy bands, density-of-states functions, and optical absorption for the samples used in this study are shown in Figs. 1 and 2.

In the Anderson model, conduction-band states acquire a homogeneous linewidth due to the mixing between the localized defect states and the extended band states. The density of states in the restructured conduction bands has been calculated by Wu *et al.* [2] using Green's function techniques:

$$\rho(E_k^{\pm}) = \frac{1}{\pi}\int_{\text{band}} \rho_0(E_{k'}^c)\text{Im}[G(E_k^{\pm}, E_{k'}^c)]dE_{k'}^c, \qquad (2)$$

where $\text{Im}[G(E_k^{\pm}, E_{k'}^c)]$ is the imaginary part of the Green's function

$$G_{kk}(E_k^{\pm}, E_{k'}^c) = \left[E_k^{\pm} - E_{k'}^c - \frac{V^2 x}{E_k^{\pm} - E_{\text{N}} - i\pi V^2 \beta\rho_0(E_{\text{N}})}\right]^{-1}. \qquad (3)$$

Here, $\rho_0(E_k^c)$ is the density of states in the unperturbed conduction band, $\rho_0(E_{\text{N}})$ is the unperturbed density of states at the nitrogen defect-state energy, and β is a constant of order 1. In our samples, the defect energy E_{N} lies just above (S205B) or below (S376B) the unperturbed conduction-band edge. Since the unperturbed density of states vanishes at the band edge, $\rho_0(E_{\text{N}}) \ll 1$ $(\text{unit cell eV})^{-1}$ for both samples. We successfully fit our optical absorption measurements [Figs. 1(c) and 2(c)] with our model for values of $\beta\rho_0(E_{\text{N}}) < 0.003$, and we choose $\beta\rho_0(E_{\text{N}}) = 10^{-3}$ in the remainder of our analysis. The valence-band density of states is calculated in spherical parabolic band approximation.

Our samples consist of a $GaP_yAs_{1-x-y}N_x$ layer grown on a series of GaP_yAs_{1-y} layers on a GaP substrate. The optical absorbance is computed as the sum of the absorbance in each layer of the sample:

$$a(E_J) = \alpha_{\text{N}}(E_J)d_{\text{N}} + \sum_i \alpha_{\text{GaP}_{(1-y_i)}\text{As}_{y_i}}(E_J)d_i + \alpha_{\text{GaP}}(E_J)d_{\text{substrate}}, \qquad (4)$$

where E_J is the transition energy. The first term on the right-hand side represents the nitrogen-doped layer; the second term is a sum over the GaP_yAs_{1-y} layers. The last term is the substrate absorption. Absorption in the GaP_yAs_{1-y} layers is assumed to be proportional to the joint density of states calculated in the effective mass

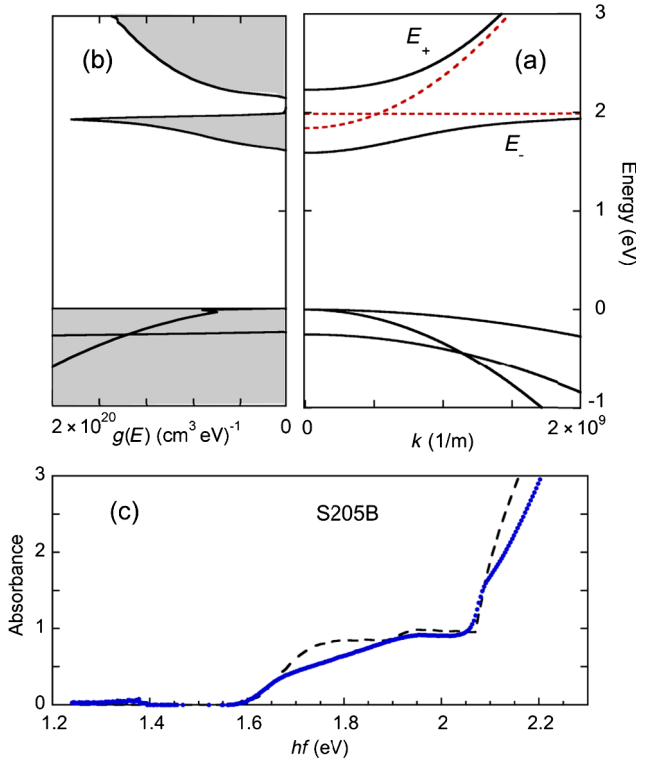

FIG. 1. (a) Model energy-band diagram for $GaP_yAs_{1-x-y}N_x$ sample S205B ($x = 1.2\%$, $y = 33\%$) from the band anticrossing model (solid lines). Dashed lines show the unperturbed conduction band and N-defect level. (b) Density of states versus energy. (c) Optical absorbance versus energy. The solid line is the measured absorbance, and the dashed line is the model absorbance of the sample and the substrate.

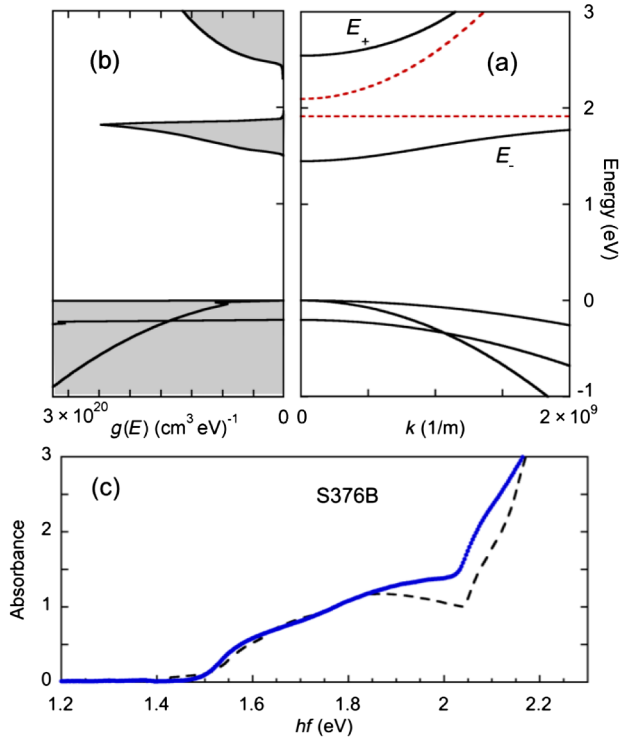

FIG. 2. (a) Model energy-band diagram for $GaP_yAs_{1-x-y}N_x$ sample S376B ($x = 3.6\%$, $y = 49\%$) from the band anticrossing model (solid lines). Dashed lines show the unperturbed conduction band and N-defect level. (b) Density of states versus energy. (c) Optical absorbance versus energy. The solid line is the measured absorbance, and the dashed line is the model absorbance of the sample and the substrate.

TABLE I. BAC model parameters used for the two samples investigated in this work. Energies are relative to the valence-band maximum.

Sample	x	y	V (eV)	E_N (eV)	$\beta\rho_0(E_N)$ (eV^{-1})
S205B	1.2%	33%	2.4	1.988	10^{-3}
S376B	3.6%	49%	2.4	1.915	10^{-3}

approximation, with the proportionality constant determined by fitting the near-band-edge absorption in GaAs. Absorption in the substrate is modeled using published optical constants for GaP [22].

The optical absorbance in the $GaP_yAs_{1-x-y}N_x$ layer is calculated using the BAC model following the procedure described by Wu [2]. Although the nitrogen defect states are localized and randomly distributed, k conservation is restored in the coherent potential approximation. The absorption coefficient is

$$\alpha_N(E_J) = \frac{C}{E_J}\sum_v\sum_{+,-}\rho_J(E_J^{\pm})|M|^2(1-f_k^{v,h}-f_k^{\pm,e}), \quad (5)$$

where C is a constant, $f_k^{v,h}$ is the hole occupancy of state k in the valence band v, $E_J^{\pm}$ is the transition energy to the E_+ or E_- band, and $f_k^{\pm,e}$ is the electron occupancy of state k in the E_+ or E_- band. The joint density of states for the transitions is calculated to be

$$\rho_J(E_J^{\pm}) = \int_{\text{band}} \rho(E_k^{\pm})\delta(E_J - E_k^{\pm} + E_k^v)dE_k^c. \quad (6)$$

The matrix elements for the transition are determined by the localized and extended components of the electron wave functions. Perturbation theory yields

$$\begin{aligned} M_{v,E_+} &= \cos(\theta/2)M_{v,c} + \sin(\theta/2)M_{v,N}, \\ M_{v,E_-} &= -\sin(\theta/2)M_{v,c} + \cos(\theta/2)M_{v,N}, \\ M_{E_+,E_-} &= [\cos^2(\theta/2) - \sin^2(\theta/2)]M_{c,N}, \end{aligned} \quad (7)$$

where $\tan(\theta) = (2V/E_k^c - E_N)$, $M_{v,c}$ is the optical matrix element between valence band v and the unperturbed conduction band c, and $M_{v,N}$ and $M_{c,N}$ are matrix elements between the band states and the nitrogen defect state. Figures 1 and 2 show good agreement between the model and experiment by treating the nitrogen fraction of each sample as an adjustable parameter and assuming $M_{v,N} \ll M_{v,c}$.

Induced absorption between E_- and E_+ should be observable after the optical population of the intermediate band. For optical transitions that conserve energy and momentum, we should find

$$\alpha_N(E_J) = \frac{D}{E_J}\rho_J(E_J^{\pm})|M_{E+,E-}|^2(f_k^{-,e} - f_k^{+,e}), \quad (8)$$

where D is a constant. As we discuss below, we observe induced absorption in one sample that cannot be fit by Eq. (8), suggesting it arises from intermediate- to conduction-band transitions that do not conserve k. We model this absorption as a spectrally featureless absorption process, $\alpha \propto n_-/E_j^2$.

III. EXPERIMENT

Epitaxial $GaP_yAs_{1-x-y}N_x$ layers are grown [19] in a Varian Gen II molecular-beam-epitaxy system modified to handle gas phase AsH_3 and PH_3. Starting at the GaP substrate, a 0.3-μm GaP buffer layer is grown at 580 °C, followed by a 1.5-μm-thick linearly graded GaP_yAs_{1-y} layer in which y increases from zero to the final composition, and then by a 0.5-μm-thick GaP_yAs_{1-y} layer grown at 520 °C. The 0.5-μm $GaP_yAs_{1-x-y}N_x$ active layer is then grown at 520 °C using rf-plasma-activated N. The sample structure is confirmed by Rutherford backscattering, which determines the concentrations of Ga, As, and P as a function of depth. For S205B, the N concentration in a sample from the same wafer is measured to be $x = 1.5\%$ by nuclear-reaction analysis using the $^{14}N(\alpha, p)^{17}O$ reaction with a 3.72-MeV $^4He^2$ beam. This result is close to the value ($x = 1.2\%$) obtained by fitting the optical absorption in our sample.

The samples for optical measurements are mounted episide down on quartz slides with optical epoxy, and the substrates are thinned to approximately 20 μm. Transmission and reflectance measurements are performed with a Perkin-Elmer 950 UV/Vis/NIR spectrophotometer to determine the absorbance over the spectral range 1.0–2.5 eV. The measured absorbance of each sample is compared to the simulated absorbance in a model structure [Figs. 1(c) and 2(c)].

Optical pump and optical probe transient absorption measurements of these samples are performed using a HELIOS transient absorption system (Ultrafast Systems). In this system, a 1-KHz repetition rate amplified femtosecond Ti-sapphire laser (Coherent Evolution) creates approximately 5-mJ 100-fs pulses centered at $\lambda \sim 800$ nm. The pulses are divided at a beam splitter to generate a tunable pump pulse in an optical parametric amplifier and a supercontinuum white-light probe pulse. The white-light pulse is further divided into a sample pulse and a reference pulse. The pump pulse propagates through a delay stage and uniformly illuminates the region of the sample interrogated by the sample pulse. The pump beam spot diameter is approximately 0.3 mm, and the probe beam diameter is approximately 0.05 mm. Pump-pulse photon energies of 1.91 eV (650 nm) and 2.82 eV (440 nm) are used, and the measurements are recorded at pump intensities ranging from approximately 0.5 to 5 mJ/cm^2. The sample and reference pulses

are recorded by separate CCD spectrographs allowing transmission spectra to be obtained for each laser pulse. An optical chopper blocks alternate pump pulses to determine the change in the transmission spectrum of the sample due to the pump as a function of the delay between the pump and probe pulses. Transient absorption spectra are recorded in the visible spectral range (1.5–2.5 eV) and the near-infrared spectral range (0.8–1.5 eV) in separate experiments using independent systems.

IV. RESULTS

Figures 3(a) and 3(b) summarize the transient absorption data for sample S205B ($GaP_{0.33}As_{0.66}N_{0.012}$). We discuss our model spectra [Fig. 3(c)] in the next section. In this measurement, the pump photon energy is 2.82 eV, and the pump intensity is approximately 1 mJ/cm^2. The spectra show an optically induced *decrease* in absorption at probe photon energies $hf > 1.6$ eV and an *increase* in absorption at energies $hf < 1.5$ eV. The absorption saturation observed at $hf > 1.6$ eV contains two distinct bands with maxima at 1.7 and 2.25 eV. A third, partially resolved band is observed at 1.9 eV. The induced absorption at $hf < 1.5$ eV is stronger at low frequencies but shows no other spectral features. Figures 4(a) and 4(b) summarize the transient absorption data for sample S376B ($GaP_{0.49}As_{0.474}N_{0.036}$). The results are qualitatively similar, with an optically induced *decrease* in absorption at probe photon energies $hf > 1.5$ eV and an *increase* in absorption at energies $hf < 1.5$ eV. We do not observe a distinct higher-energy band in the transient absorption spectrum of S376B within the experimentally accessible range set by substrate absorption, $hf < 2.4$ eV.

Our measurements also probe the dynamics of the transient absorption signal. For pump excitation at $hf = 2.82$ eV (440 nm) in sample S205B [see Fig. 3(b)], the absorption change builds up over approximately 1 ps following photoexcitation and decays on a time scale of 10–100 ps. The spectrum of the transient absorption decrease at $hf > 1.6$ eV narrows toward lower frequency with increasing delay. For pump excitation at $hf = 1.91$ eV (650 nm, not shown) the absorption change builds up faster, reaching its maximum value approximately 0.3 ps

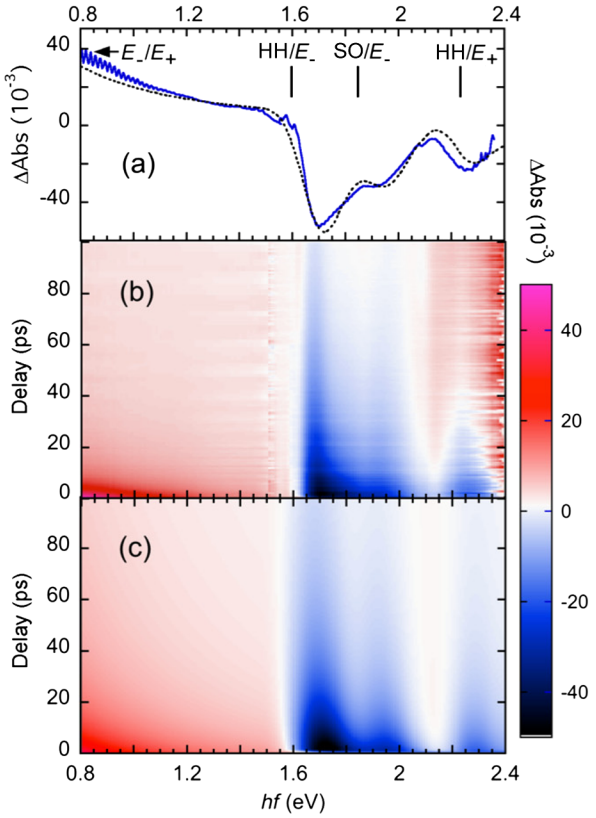

FIG. 3. Transient absorbance of sample S205B. (a) Absorbance change 2 ps after optical excitation. Solid line is the measurement, while the dashed line is our model. Markers show onset energies for interband transitions. The E_--E_+ onset is outside the measured range. (b) Measured absorbance change for pump-probe delays of 0–100 ps. (c) Model prediction.

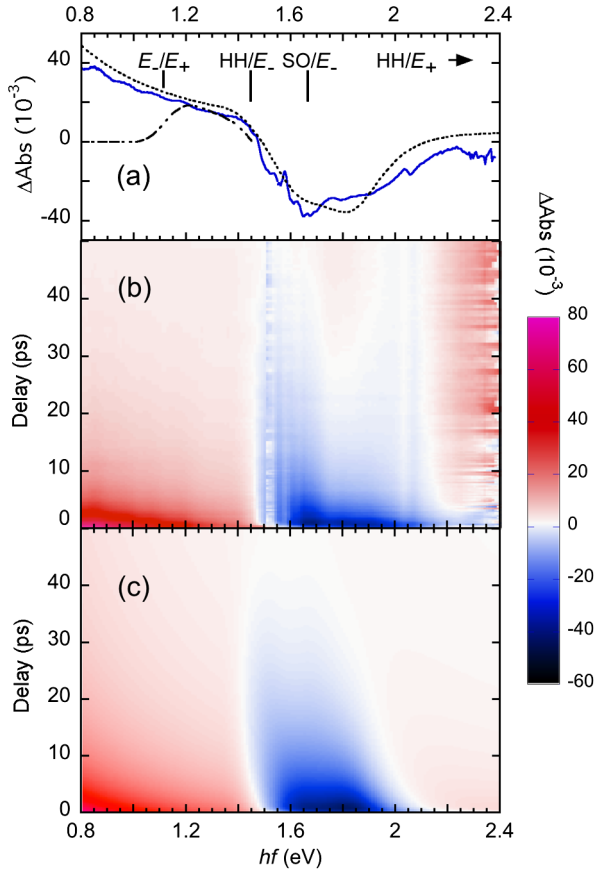

FIG. 4. Transient absorbance of sample S376B. (a) Absorbance change 2 ps after optical excitation. Solid line is the measurement, dotted line is our model, dashed line is a model including only k-conserving E_-/E_+ transitions. Markers show onset energies for interband transitions. The HH-E_+ transition is outside the measured range. (b) Measured absorbance change for delays of 0–50 ps. (c) Model prediction.

after the pump pulse, and the transient absorption signal is concentrated at lower frequencies. Similar trends are observed in the transient absorption spectra of sample S376B ($GaP_{0.49}As_{0.47}N_{0.036}$) [Fig. 4(b)].

V. DISCUSSION

We model the transient absorption by fitting valence-, intermediate-, and conduction-band populations and a single-carrier temperature $T_e = T_h$ at each moment in time. Carrier populations in optically excited *III-V* semiconductors thermalize in tens of femtoseconds [23], much faster than the time scale investigated here. We assume thermalized (Fermi-Dirac) carrier distributions in each band, find the distribution functions, and calculate the optical absorption using Eq. (4). In addition, because the strength of the E_--E_+ absorption depends on a matrix element $M_{c,N}$ not determined by our equilibrium measurements, the ratio of the induced absorption strength to the intermediate-band population is used as an adjustable parameter for each sample.

The model fits the transient absorption data for sample S205B well [Fig. 3(a)]. Saturated absorption features are observed just above the onset energies predicted for the heavy-hole to E_- transition (HH-E_-), the split-off-band to E_- transition (SO-E_-), and the heavy-hole to E_+ transition (HH-E_+). The induced absorption observed at $hf <$ 1.5 eV is consistent with the E_--E_+ transition. For sample S376B [Fig. 4(a)], the model predicts the observed decrease in absorption at $hf = 1.4$–2 eV due to saturation of the VB-E_- transition. Distinct features consistent with the SO-E_- transition are apparent in the experimental data but are only barely visible in the simulation. The model also predicts saturation of the VB-E_+ transition at $hf = 2.5$ eV, but this is inaccessible due to substrate absorption. Induced absorption between the E_--E_+ bands is predicted at $hf = 1.1$–1.5 eV. However, the experimentally induced absorption does not cut off below 1.1 eV, as predicted for transitions that conserve k. Instead, we fit the induced absorption in both samples by assuming $\alpha \propto n_-/E_j^2$, indicating that the induced absorption is proportional to the population of the intermediate band.

The transient absorption evolves due to carrier redistribution within the bands and carrier recombination. The model fits match the evolution of the transient absorption well for S205B [Fig. 3(c)]. For S376B, the model fit is spectrally smoother than the experimental data [Fig. 4(c)], and the features associated with the SO-E_- transition are not distinct in the simulation. Despite this discrepancy, the data still strongly constrain the best-fit intermediate-band population for this sample. We use these fits to extract electron concentrations in the E_+ and E_- bands and the carrier temperature at each delay value for each sample. The intermediate- and conduction-band populations in sample S205B extracted from these fits are plotted in Fig. 5. For pump irradiance $I \leq 1$ mJ/cm^2, we find the conduction-band population to decay exponentially with time. We extract the time constant $\tau_{E+-E-} = 23$ ps for electron relaxation from the conduction band to the intermediate band using a coupled-rate-equation system. At higher pump irradiance, the conduction-band population decays faster, and the decay is nonexponential. In contrast, the electron population in the intermediate band does not decay exponentially but instead fits a bimolecular recombination process $dn(E_-)/dt = -r[n(E_-)p]$, where r is the recombination constant and $p = n(E_-) + n(E_+)$. A plot of $dn(E_-)/dt$ t versus $n(E_-)p$ for the full range of pump intensities investigated (inset, Fig. 5) yields $r = 2.3 \times 10^{-8}$ cm^3/s. Figure 6 shows the intermediate-band population versus time for sample S376B. The intermediate-band dynamics also fit a bimolecular recombination process, although the value of the recombination constant depends on our model for the (unobserved) conduction-band population. Assuming a similar exponential decay of the conduction-band population in S376B as in S205B yields $r = 3.5 \times 10^8$ cm^3/s. Bimolecular recombination in semiconductors is often associated with radiative recombination, but radiative r values are typically approximately 100 times smaller than those observed here. We estimate $r_{\text{radiative}} = 3 \times 10^{-10}$ cm^3/s for S205B using the van Roosbroeck–Shockley relation [24]. We suggest that trap-mediated recombination is responsible for the higher recombination rates observed in our samples.

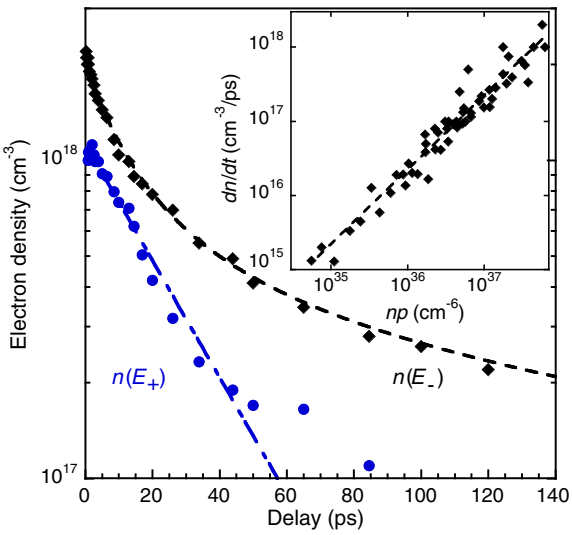

FIG. 5. Carrier population versus time for sample S205B from model fits to the transient absorption versus delay at pump intensity of 1 mJ/cm^2. Black diamonds: intermediate-band population $n(E_-)$. Black dashed line is a bimolecular recombination model. Blue circles: conduction-band population $n(E_+)$. Blue dashed line is an exponential decay model. Inset: rate of change of $n(E_-)$ versus $n(E_-)p$. Points are obtained from measured carrier populations for pump intensities 0.5–5 mJ/cm^2. Linear fit (dashed line) is the bimolecular recombination model.

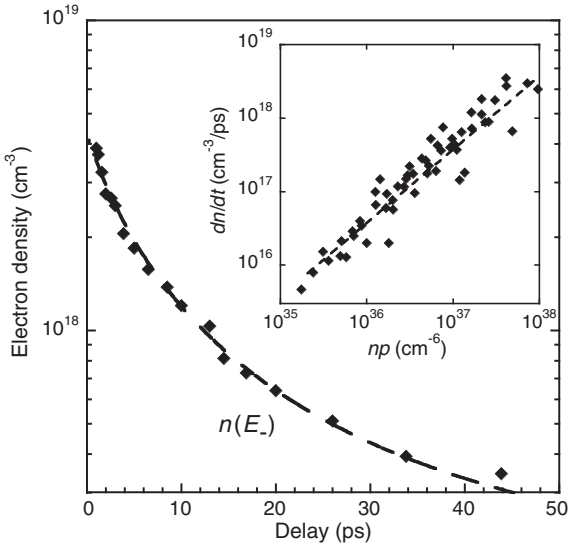

FIG. 6. Carrier population versus time for sample S376B measured at pump intensity of 1 mJ/cm^2. Black diamonds: intermediate-band population $n(E_-)$ versus delay. Black dashed line is a bimolecular recombination model. Inset: rate of change of $n(E_-)$ versus $n(E_-)p$. Points are obtained from measured carrier populations for pump intensities 0.5–5 mJ/cm^2. Linear fit (dashed line) is the bimolecular recombination model.

The approximately 1-ps buildup time of the transient absorption signal arises from hot carrier effects. The carrier temperature following photoexcitation versus delay for sample S205B is shown in Fig. 7. We find a carrier temperature of 2160 K at 0.2 ps after photoexcitation. The carriers initially cool rapidly, reaching 500 K at 1 ps and 400 K at 2.6 ps. Our data can be described well by a cooling curve calculated for hot carriers in GaAs by Shah [23] (see Fig. 7), where we shift the origin of the time axis for the calculated cooling curve by 0.3 ps to match our higher initial temperature. In GaAs, hot carriers rapidly cool by optical phonon emission until the carrier kinetic energies drop below the optical phonon energy. Carrier cooling in our $GaP_yAs_{1-x-y}N_x$ samples appears to follow a similar process.

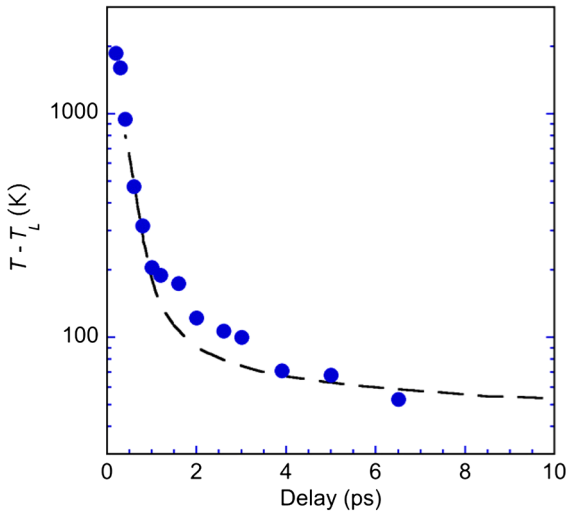

FIG. 7. Temperature difference between the electron gas and the lattice versus time after optical excitation for sample S205B measured at pump intensity of 1 mJ/cm^2. Points are obtained from model fits to the transient absorbance. Black dashed line is a calculated cooling curve for electrons in GaAs [23].

As noted above, for sample S376B, the induced absorption does not cut off below the energy of the smallest k-conserving interband transition predicted by our model. This leads us to consider two other mechanisms for the induced absorption: free-carrier absorption by the photoexcited holes and non-k-conserving E_--E_+ transitions by the electrons. Note that intraband absorption by free *electrons* cannot be responsible for the induced absorption because the transition energies exceed the width of the intermediate band. It is clear that intraband (Drude) and intervalence-band transitions by optically excited holes will produce absorption. These processes have been studied in p-type bulk *III-V* semiconductors [25,26], and they produce weak optical absorption with $\alpha \propto n/E^2$ in the spectral region $hf = 0.8$–1.5 eV. However, the induced absorption in S205B and S376B is too strong to be explained by this mechanism. Intervalence-band absorption varies with the hole density, while Drude absorption depends on both the carrier density and momentum scattering time. For hole densities predicted by our model, there is no scattering time that produces free-hole absorption larger than approximately 10% of the observed induced absorption. In contrast, weaker induced absorption observed in our reference samples [GaP_yAs_{1-y} samples with no nitrogen doping, not shown] in the IR spectral range is consistent with free-carrier absorption.

Alternately, we suggest that non-k-conserving interband transitions of electrons between E_- and E_+ contribute to the optical absorption. The energy range of all possible interband transitions extends down to the E_--E^+ band gap, which is below the experimentally accessible spectral range for both samples. We speculate that disorder in our samples may relax k conservation for E_--E^+ optical transitions. Transitions near the E_--E^+ band gap also involve initial and final states that have the highest contribution from the localized nitrogen orbitals and, thus, most strongly violate the coherent potential approximation. We conclude that our data are consistent with this mechanism.

Finally, we compare our measured lifetimes to those required for a practical $GaP_yAs_{1-x-y}N_x$ intermediate-band solar cell. The conduction-band lifetime must be large enough so that the photocarrier diffusion length exceeds the absorber layer thickness. An order of magnitude estimate yields a minimum lifetime $\tau_{E+} \sim 400$ ps using a carrier mobility $\mu \sim 1000$ cm^2/V s and a layer thickness of $d \sim 1$ μm. In addition, the intermediate-band lifetime must be long enough so that electrons promoted to the

intermediate band can be photoexcited to the conduction band before they recombine [27,28]. An order of magnitude estimate yields $\tau_{E-} \sim 20$ μs, approximately 5 orders of magnitude larger than our measured intermediate-band recombination time. We estimate the minimum lifetime from the average time for photoexcitation out of the intermediate band, $\tau_G = n(E_-)/\phi\alpha$, where α is the absorption coefficient for intermediate- to conduction-band transitions, and ϕ is the solar photon flux in the relevant spectral range (0.8–1.5 eV in S205B). We assume that the intermediate-band solar cell is likely to be doped to place the Fermi level in the middle of the intermediate band, $n(E_-) \sim 10^{19}$ cm^{-3}, and we estimate $\alpha \sim 5000$ cm^{-1} for this case by extrapolation from our transient absorption results. We also assume $\phi \sim (2 \times 10^{17}$ cm^{-2} s$^{-1})C$, and take $C \sim 500$ for the maximum practical concentration factor. A similar discrepancy between the required and measured intermediate-band lifetimes has been observed in quantum-dot-based IBSCs [28].

The present results identify the short minority-carrier lifetime in our samples as the factor responsible for low efficiency of intermediate-band solar cells and also provide guidance on ways to address this issue. Since the carrier recombination is most likely controlled by defects rather than by intrinsic processes, it may be possible to achieve longer minority-carrier lifetimes by optimizing the materials synthesis process, e.g., to reduce inhomogeneity in N doping. As it has been demonstrated for multijunction and intermediate-band solar cells [10], the minority-carrier lifetime can be greatly increased by quenching carrier recombination centers in cells operating under concentrated sunlight conditions. This is attributed to suppression of nonradiative recombination by saturation of the Shockley-Read-Hall-type defects under concentrated light conditions [29]. Also, it was shown recently [30] that the performance of a quantum-dot intermediate-band PV devices improves under high-intensity illumination. The effect was explained by changes in the occupancy of different bands induced by the dynamics of photoexcited carriers. Finally, the intermediate-band structure allows for optimization of the absorption and recombination processes as well as charge collection by varying the alloy composition and the occupancy of the intermediate band, and device structures with composition and doping gradients can be used to improve charge collection by creating strong built-in fields to rapidly extract carriers from the active layer.

V. CONCLUSIONS

We use transient absorption spectroscopy to probe carrier lifetimes in two samples of the intermediate-band semiconductor $GaP_yAs_{1-x-y}N_x$. An optical pump pulse excites electrons from the valence band to the intermediate and conduction bands, and we record absorption saturation of the VB-E_- and VB-E_+ transitions and induce absorption that we associate with the E_--E_+ transition. We model the optical properties of our samples using the band anticrossing model to extract carrier densities as a function of time. Following photoexcitation of $GaP_{0.32}As_{0.67}N_{0.012}$ (S205B) with <1 mJ/cm^2 pulses, we find that the electron population in the conduction band decays exponentially with time constant $\tau_{CB} = 23$ ps. The electron population in the intermediate band exhibits bimolecular recombination with recombination constant $r = 2 \times 10^{-8}$ cm^3/s. The measurements of $GaP_{0.54}As_{0.46}N_{0.036}$ (S376B) find that the intermediate-band electron population exhibits bimolecular recombination with recombination constant $r = 3.5 \times 10^{-8}$ cm^3/s. Although these rapid recombination processes strongly limit the efficiency of intermediate-band cells made from this material, there are several ways to improve the performance by optimizing the growth conditions and the device structure.

ACKNOWLEDGMENTS

This work is performed in the Electronic Materials Program and the Molecular Foundry at Lawrence Berkeley National Laboratory and is supported by the Office of Science, Office of Basic Energy Sciences of the U.S. Department of Energy under Contract No. DE-AC02-05CH11231. J. H. acknowledges sabbatical support from Macalester College. K. M. Y. acknowledges the support of the General Research Fund of the Research Grants Council of Hong Kong SAR, China, under Project No. CityU 11303715. The samples are synthesized in Professor Tu's laboratory at University of California, San Diego, and the experiments are carried out by J. H. and A. S. The interpretation of the experimental results is done by J. H. and W. W. The other authors contribute to the material characterization and discuss the results. The authors acknowledge the support of the Joint Center for Artificial Photosynthesis at University of California, Berkeley for transient absorption measurements using an infrared probe.

[1] W. Shan, W. Walukiewicz, J. W. Ager, E. E. Haller, J. F. Geisz, D. J. Friedman, J. M. Olson, and S. R. Kurtz, Band Anticrossing in GaInNAs Alloys, Phys. Rev. Lett. **82**, 1221 (1999).

[2] J. Wu, W. Shan, and W. Walukiewicz, Band anticrossing in highly mismatched *III-V* semiconductor alloys, Semicond. Sci. Technol. **17**, 860 (2002).

[3] W. Shan, W. Walukiewicz, K. M. Yu, J. W. Ager, E. E. Haller, J. F. Geisz, D. J. Friedman, J. M. Olson, S. R. Kurtz, and C. Nauka, Effect of nitrogen on the electronic band structure of group *III-N-V* alloys, Phys. Rev. B **62**, 4211 (2000).

[4] J. D. Perkins, A. Mascarenhas, J. F. Geisz, and D. J. Friedman, Conduction-band-resonant nitrogen-induced levels in $GaAs_{1-x}N_x$ with $x < 0.03$, Phys. Rev. B **64**, 121301 (2001).

[5] C. Skierbiszewski, P. Perlin, P. Wisniewski, W. Knap, T. Suski, W. Walukiewicz, W. Shan, K. M. Yu, J. W. Ager, E. E. Haller, J. F. Geisz, and J. M. Olson, Large, nitrogen-induced increase of the electron effective mass in $In_yGa_{1-y}N_xAs_{1-x}$, Appl. Phys. Lett. **76**, 2409 (2000).

[6] J. Wu, W. Walukiewicz, K. M. Yu, J. W. Ager, E. E. Haller, Y. G. Hong, H. P. Xin, and C. W. Tu, Band anticrossing in $GaP_{1-x}N_x$ alloys, Phys. Rev. B **65**, 241303(R) (2002).

[7] R. Kudrawiec, A. V. Luce, M. Gladysiewicz, M. Ting, Y. J. Kuang, C. W. Tu, O. D. Dubon, K. M. Yu, and W. Walukiewicz, Electronic Band Structure of GaN_xPyAs_{1-x-y} Highly Mismatched Alloys: Suitability for Intermediate-Band Solar Cells, Phys. Rev. Applied **1**, 034007 (2014).

[8] A. Luque and A. Marti, Increasing the Efficiency of Ideal Solar Cells by Photon Induced Transitions at Intermediate Levels, Phys. Rev. Lett. **78**, 5014 (1997).

[9] A. Luque, A. Marti, and C. Stanley, Understanding intermediate-band solar cells, Nat. Photonics **6**, 146 (2012).

[10] Y. Okada, N. J. Ekins-Daukes, T. Kita, R. Tamaki, M. Yoshida, A. Pusch, O. Hess, C. C. Phillips, D. J. Farrell, K. Yoshida, N. Ahsan, Y. Shoji, T. Sogabe, and J. F. Guillemoles, Intermediate band solar cells: Recent progress and future directions, Appl. Phys. Rev. **2**, 021302 (2015).

[11] N. Lopez, L. A. Reichertz, K. M. Yu, K. Campman, and W. Walukiewicz, Engineering the Electronic Band Structure for Multiband Solar Cells, Phys. Rev. Lett. **106**, 028701 (2011).

[12] T. Tanaka, K. M. Yu, A. X. Levander, O. D. Dubon, L. A. Reichertz, N. Lopez, M. Nishio, and W. Walukiewicz, Demonstration of $ZnTe_{1-x}O_x$ intermediate band solar cell, Jpn. J. Appl. Phys. **50**, 082304 (2011).

[13] A. Luque, P. G. Linares, E. Antolin, I. Ramiro, C. D. Farmer, E. Hernandez, I. Tobias, C. R. Stanley, and A. Marti, Understanding the operation of quantum dot intermediate band solar cells, J. Appl. Phys. **111**, 044502 (2012).

[14] N. Ahsan, N. Miyashita, M. M. Islam, K. M. Yu, W. Walukiewicz, and Y. Okada, Two-photon excitation in an intermediate band solar cell structure, Appl. Phys. Lett. **100**, 172111 (2012).

[15] N. Lopez, K. M. Yu, T. Tanaka, and W. Walukiewicz, Multicolor electroluminescence from intermediate band solar cell structures, Adv. Energy Mater. **6**, 1501820 (2016).

[16] K. M. Yu, W. Walukiewicz, J. Wu, W. Shan, J. W. Beeman, M. A. Scarpulla, O. D. Dubon, and P. Becla, Diluted II-VI Oxide Semiconductors with Multiple Band Gaps, Phys. Rev. Lett. **91**, 246403 (2003).

[17] T. Tanaka, M. Miyabara, Y. Nagao, K. Saito, Q. X. Guo, M. Nishio, K. M. Yu, and W. Walukiewicz, Photocurrent induced by two-photon excitation in ZnTeO intermediate band solar cells, Appl. Phys. Lett. **102**, 052111 (2013).

[18] K. M. Yu, W. Walukiewicz, J. W. Ager, D. Bour, R. Farshchi, O. D. Dubon, S. X. Li, I. D. Sharp, and E. E. Haller, Multiband GaNAsP quaternary alloys, Appl. Phys. Lett. **88**, 092110 (2006).

[19] Y. J. Kuang, K. M. Yu, R. Kudrawiec, A. V. Luce, M. Ting, W. Walukiewicz, and C. W. Tu, GaNAsP: An intermediate band semiconductor grown by gas-source molecular beam epitaxy, Appl. Phys. Lett. **102**, 112105 (2013).

[20] M. Baranowski, R. Kudrawiec, A. V. Luce, M. Latkowska, K. M. Yu, Y. J. Kuang, J. Misiewicz, C. W. Tu, and W. Walukiewicz, Temperature evolution of carrier dynamics in $GaN_{(x)}P_{(y)}As_{(1-y-x)}$ alloys, J. Appl. Phys. **117**, 175702 (2015).

[21] W. Walukiewicz, K. M. Yu, J. Wu, J. W. Ager, E. E. Haller, I. Miotkowski, A. K. Ramdas, and C. H. Su, Band anticrossing in highly mismatched compound semiconductor alloys, Compd Semicond **2001**, 301 (2002).

[22] A. Borghesi and G. Guizzetti, in *Handbook of the Optical Constants of Solids*, edited by E. D. Palik (Academic Press, London, 1985), Vol. I, pp. 445.

[23] J. Shah, *Ultrafast Spectroscopy of Semiconductors and Semiconductor Nanostructures*, 2nd ed. (Springer, Berlin, 1999).

[24] W. Vanroosbroeck and W. Shockley, Photon-radiative recombination of electrons and holes in germanium, Phys. Rev. **94**, 1558 (1954).

[25] E. O. Kane, Energy band structure in *p*-type germanium and silicon, J. Phys. Chem. Solids **1**, 82 (1956).

[26] W. Songprakob, R. Zallen, W. K. Liu, and K. L. Bacher, Infrared studies of hole-plasmon excitations in heavily-doped *p*-type MBE-grown GaAs: C, Phys. Rev. B **62**, 4501 (2000).

[27] T. Kita, T. Maeda, and Y. Harada, Carrier dynamics of the intermediate state in InAs/GaAs quantum dots coupled in a photonic cavity under two-photon excitation, Phys. Rev. B **86**, 035301 (2012).

[28] G. Jolley, L. Fu, H. F. Lu, H. H. Tan, and C. Jagadish, The role of intersubband optical transitions on the electrical properties of InGaAs/GaAs quantum dot solar cells, Prog. Photovoltaics **21**, 736 (2012).

[29] M.-j. Yang and Y. Masafumi, Properties of GaAs/InGaAs quantum well solar cells under low concentration operation, Sol. Energy Mater. Sol. Cells **60**, 19 (2000).

[30] T. Sogabe, Y. Shoji, M. Ohba, K. Yoshida, R. Tamaki, H. Hwen-Fen, C.-H. Wu, C.-T. Kuo, S. Tomic, and Y. Okada, Intermediate-band dynamics of quantum dots solar cell in concentrator photovoltaic modules, Sci. Rep. **4**, 4792 (2014).